

Half-integer Shapiro steps in MgB_2 focused He ion beam Josephson junctions

Dali Yin(殷大利), Xinwei Cai(蔡欣炜), Tiequan Xu(徐铁权), Ruining Sun(孙瑞宁), Ying Han(韩颖), Yan Zhang(张焱), Yue Wang(王越), and Zizhao Gan(甘子钊)
Citation: Chin. Phys. B, 2024, 33 (**8**): 087404. DOI: 10.1088/1674-1056/ad4d62

What follows is a list of articles you may be interested in

Co-doped $BaFe_2As_2$ Josephson junction fabricated with a focused helium ion beam

Ziwen Chen(陈紫雯), Yan Zhang(张焱), Ping Ma(马平), Zhongtang Xu(徐中堂), Yulong Li(李宇龙), Yue Wang(王越), Jianming Lu(路建明), Yanwei Ma(马衍伟), and Zizhao Gan(甘子钊)
Chin. Phys. B, 2024, 33 (**4**): 047405. DOI: 10.1088/1674-1056/ad21f7

Anomalous spin Josephson effect in spin superconductors

Wen Zeng(曾文) and Rui Shen(沈瑞)
Chin. Phys. B, 2024, 33 (**3**): 037401. DOI: 10.1088/1674-1056/ad1982

Josephson vortices and intrinsic Josephson junctions in the layered iron-based superconductor $Ca_{10}(Pt_3As_8)((Fe_{0.9}Pt_{0.1})_2As_2)_5$

Qiang-Tao Sui(随强涛) and Xiang-Gang Qui(邱祥冈)
Chin. Phys. B, 2022, 31 (**9**): 097403. DOI: 10.1088/1674-1056/ac76ae

Asymmetric Fraunhofer pattern in Josephson junctions from heterodimensional superlattice V_5S_8

Juewen Fan(范珏雯), Bingyan Jiang(江丙炎), Jiaji Zhao(赵嘉佶), Ran Bi(毕然), Jiadong Zhou(周家东), Zheng Liu(刘政), Guang Yang(杨光), Jie Shen(沈洁), Fanming Qu(屈凡明), Li Lu(吕力), Ning Kang(康宁), and Xiaosong Wu(吴孝松)
Chin. Phys. B, 2022, 31 (**5**): 057402. DOI: 10.1088/1674-1056/ac5d30

Ac Josephson effect in Corbino-geometry Josephson junctions constructed on Bi_2Te_3 surface

Yunxiao Zhang(张云潇), Zhaozheng Lyu(吕昭征), Xiang Wang(王翔), Enna Zhuo(卓恩娜), Xiaopei Sun(孙晓培), Bing Li(李冰), Jie Shen(沈洁), Guangtong Liu(刘广同), Fanming Qu(屈凡明), and Li Lü(吕力)
Chin. Phys. B, 2022, 31 (**10**): 107402. DOI: 10.1088/1674-1056/ac89d4

Half-integer Shapiro steps in MgB_2 focused He ion beam Josephson junctions

Dali Yin(殷大利), Xinwei Cai(蔡欣炜)†, Tiequan Xu(徐铁权), Ruining Sun(孙瑞宁), Ying Han(韩颖), Yan Zhang(张焱)‡, Yue Wang(王越), and Zizhao Gan(甘子钊)

Applied Superconductivity Center, State Key Laboratory for Mesoscopic Physics, School of Physics, Peking University, Beijing 100871, *China*

(Received 17 February 2024; revised manuscript received 15 May 2024; accepted manuscript online 20 May 2024)

Half-integer microwave induced steps (Shapiro steps) have been observed in many different Josephson junction systems, which have attracted a lot of attention because they signify the deviation of current phase relation (CPR) and uncover many unconventional physical properties. In this article, we first report the discovery of half-integer Shapiro steps in MgB_2 focused He ion beam (He-FIB) Josephson junctions. The half-integer steps' dependence on microwave frequency, temperature, microwave power, and magnetic field is also analyzed. We find that the existence of half-integer steps can be controlled by the magnetic field periodically, which is similar to that of high temperature superconductor (HTS) grain boundary junctions, and the similarity of the microstructures between gain boundary junctions and He-FIB junctions is discussed. As a consequence, we mainly attribute the physical origin of half-integer steps in MgB_2 He-FIB junctions to the model that a He-FIB junction is analogous to a parallel junctions' array. Our results show that He-FIB technology is a promising platform for researching CPR in junctions made of different superconductors.

Keywords: Josephson junction, half-integer Shapiro steps, MgB_2, focused helium ion beam

PACS: 74.78.–w, 03.75.Lm, 41.85.Ar **DOI:** 10.1088/1674-1056/ad4d62

1. Introduction

Josephson junctions are important quantum devices, not only for their broad application prospects in quantum computing and wireless communication but also for their fundamental profound physics. The alternate current (AC) Josephson effect[1] is one of the most attractive properties of Josephson junctions because it demonstrates the law of phase φ change over time under a finite voltage and is a manifestation of macroscopic quantum interference. As a direct result of the AC Josephson effect, constant voltage steps, which are also named Shapiro steps,[2] will appear in current I versus voltage V curves under radio-frequency (RF) radiation. Ordinary integer Shapiro steps always appear at the voltage of $2eV/h = nf$ ($n = 0$, ±1, ±2 and so on), which originates from the phase lock between Josephson oscillation and the nth harmonic of external microwave. Here, e is electron charge, h is Planck constant, and f is external microwave frequency.

Remarkably, half-integer ($n = \pm p/2$) and even fractional ($n = \pm p/q$) Shapiro steps have been observed and researched in various Josephson junction systems in the past few decades, including InAs and graphene highly transmissive Josephson junctions,[3–7] superconductor–ferromagnet–superconductor (SFS) junctions,[8–13] complex Josephson junction networks,[14–19] and high temperature superconductor (HTS) grain boundary junctions.[20–23] Although the specific physical origin of the half-integer steps in each junction system is different, the current phase relation (CPR) in these junction systems is skewed from sinusoidal form to non-sinusoidal form with higher harmonic terms.[24] Furthermore, experiments and theories have pointed out that some crucial parameters can control the skewness of CPR, such as gate voltage,[25] thickness of ferromagnet layer,[26,27] magnetic field,[15,28] temperature, and power of radiation.[29]

Recently, a state-of-the-art technology-focused He ion beam irradiation (He-FIB) has been used to fabricate high quality Josephson junctions in various superconducting materials, including $YBa_2Cu_3O_{7-\delta}$,[30,31] MgB_2,[32] $Bi_2Sr_2CaCu_2O_{8+x}$,[33] NbN,[34] NbTiN,[35] and Co-doped $BaFe_2As_2$,[36] which shows a great potential in applied and basic scientific research. In this work, MgB_2 He-FIB Josephson junctions of different irradiation doses and junction widths have been fabricated. In both junctions, we observe clear half-integer Shapiro steps, which is the first time reported in He-FIB junctions. Then, the influences of RF frequency, temperature, RF radiation power, and magnetic field on the half-integer steps are investigated. Finally, the physics origin of half-integer steps in the He-FIB junctions is also discussed.

2. Experiments and methods

To fabricate MgB_2 He-FIB Josephson junctions, high quality MgB_2 superconducting thin films around 30 nm were firstly deposited by hybrid physical-chemical vapor deposition (HPCVD)[37] technique on SiC (0001) substrates. Then, bilayers of Ti/Ag (5 nm/200 nm) were deposited on these films

†Corresponding author. E-mail: xwcai@pku.edu.cn
‡Corresponding author. E-mail: zhang_yan@pku.edu.cn

© 2024 Chinese Physical Society and IOP Publishing Ltd

by DC magnetron sputtering as electrical bonding pads. To prevent Ti/Ag bilayers from covering the junction areas and causing a short circuit, a metal mask was used here to occlude junction areas from metal sputtering. In the next step, the samples with 2–4 μm wide microbridges were defined by standard UV lithography and Ar ion milling. Finally, Josephson junctions were created by a single line of 30 kV He ion beam scanning across these microbridges in the Zeiss Orion Plus helium ion microscope. The process diagram before He-FIB irradiation is shown in Fig. 1 and the details of He-FIB technology will be introduced in the next section. Measurements of the samples' electrical transport properties under different temperatures, power of radiation and magnetic fields were performed in a physical properties measurement system (PPMS, Quantum Design) with the four-probe method. Here, a Keithley Model 2400 SourceMeter and a Keithley Model 2182A Nanovoltmeter were used as external current source and voltmeter. The RF signal was generated by a microwave signal source with frequency range 9.5–10.5 GHz and was applied on the junction by a rectangular antenna installed at the end of a coaxial line.

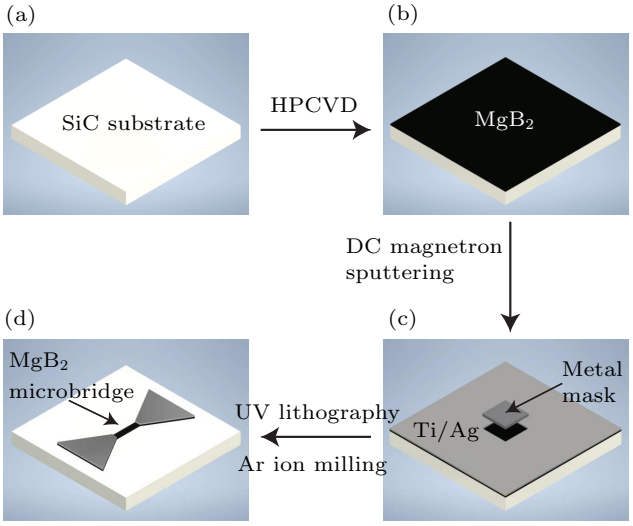


Fig. 1. Schematic diagram of the MgB_2 Josephson junction fabrication process before He-FIB irradiation, including thin films growth, sputtering Ag electrical bonding pads, lithography, and etching.

3. Results

Figure 2(a) is a schematic diagram of a junction fabricated by He-FIB, where the red cylinder represents the He-FIB with a beam diameter of 0.5 nm and the black microstrip represents a MgB_2 microbridge. The ion beam irradiates across the microbridge and creates a junction barrier, producing a Josephson junction. Figure 2(b) is the optical microscope photograph under bottom light and the black line is the ion injection effect on the substrate, which indicates the irradiation area. In this article, we report our experimental data of two MgB_2 He-FIB Josephson junctions. Junction 1 is a 2 μm wide junction with irradiation dose of 4000 ions/nm and junction 2 is a 4 μm wide junction with irradiation dose of 5000 ions/nm. Figure 2(c) shows the resistance R versus temperature T curves of these two junctions, from which we can obtain the T_c and resistance at T_c^{onset} of junction 1(39.4 K and 9.45 Ω) and junction 2 (39.8 K and 2.89 Ω). The inset in Fig. 2(c) is a close-up view of R–T curves, from which clear foot-like structures induced by thermally activated phase slippage effect[38] can be observed. The voltage V versus current I curves and differential resistance dV/dI versus current I curves at 2 K are sketched in Fig. 2(d) and its inset, from which critical current I_c and resistance at normal state R_n of junction 1 (7.02 mA and 0.30 Ω) and junction 2 (8.08 mA and 0.24 Ω) can be extracted. The detailed information of these two junctions is listed in Table 1.

For both junctions, the I_c at 2 K is too large to be suppressed by microwave radiation in our equipment and it is hard to see any Shapiro steps. However, when a specific magnetic field is applied perpendicular to the junction and the I_c is suppressed smaller than 2 mA, both junctions exhibit clear Shapiro steps under microwave radiation. Without special instructions, all following measurements are executed under a frequency $f = 10$ GHz microwave radiation and the test temperature is 2 K. Other experimental information here is that junctions 1 and 2 are both tested under 27.5 Oe magnetic field while the radiation power is 10 dBm for junction 1 and 14 dBm for junction 2. The I–V curves and dV/dI–V curves of junctions 1 and 2 are sketched in Figs. 3(a) and 3(c). Here, the horizontal ordinate n is the normalized voltage that equals to the voltage divided by $hf/(2e)$, which is around 20.7 μV for 10 GHz RF signal. In I–V curves, we can see clear constant voltage steps that are so-called Shapiro steps. The position of Shapiro steps can be extracted more precisely by the local minimums in dV/dI–V curves. The Shapiro steps appear at quantized normalized voltage values n, which are orders of them. It is worth noting that not only integer steps for $n = \pm 1$, ± 2 and ± 3 orders but also half-integer steps for $n = \pm 1/2$ and $\pm 3/2$ orders can be clearly observed. Integer steps are labeled by blue solid vertical lines and half-integer steps are labeled by green dashed vertical lines in Figs. 3(a) and 3(c). Unlike integer steps that exist clearly until very high orders, half-integer steps quickly disappear as the orders increase and can no longer be observed above $n = \pm 5/2$ orders. dV/dI–V curves under different frequenciess' radiation of junctions 1 and 2 are shown in Figs. 3(b) and 3(d), which are vertically shifted for clarity. Half-integer Shapiro steps under 9.5 GHz, 10 GHz and 10.5 GHz microwave radiation appear in both two junctions, which proves that the existence of half-integer Shapiro steps is robust and reproducible. The blue dashed fan-like lines here illustrate that as the frequency rises up, the voltage values of corresponding steps increase, which agrees with the formula that $V = nhf/(2e)$.

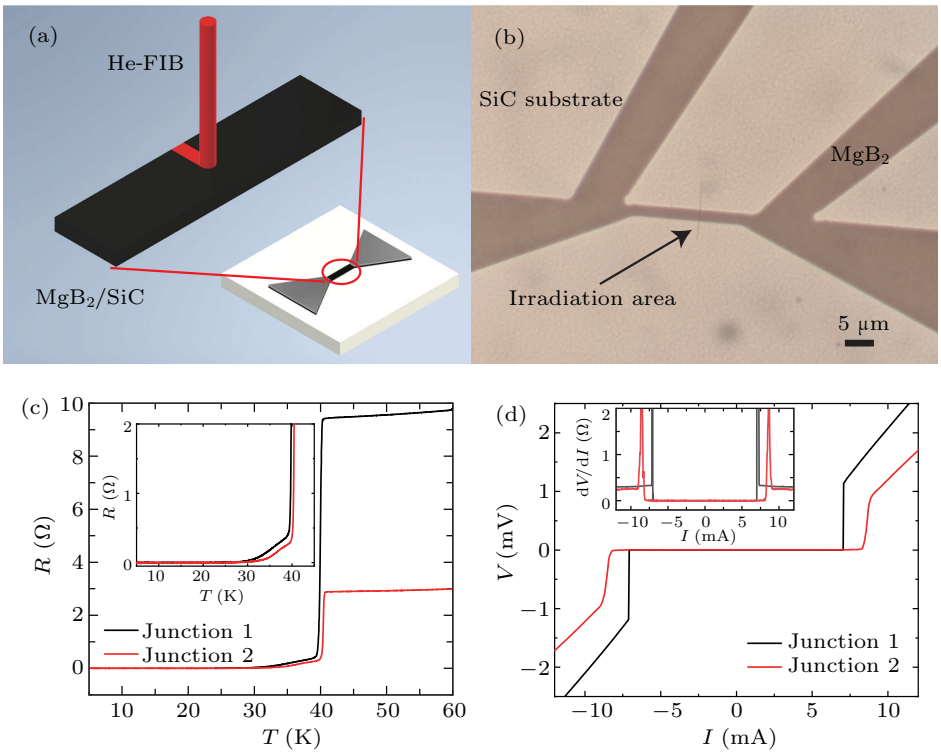


Fig. 2. (a) Schematic diagram of a MgB_2 Josephson junction fabricated by He-FIB. (b) Optical microscope photograph under bottom light where black line indicates irradiation trace. (c) R–T curves of junctions 1 and 2, where the inset is a close-up view. (d) V–I curves of junctions 1 and 2 at 2 K, where the inset shows the $\mathrm{d}V/\mathrm{d}I$–I curves.

Table 1. Detailed parameters of the junctions.

Junction number	Junction width (μm)	Dose (ions/nm)	Critical current (mA)	Resistance at normal state (Ω)
Junction 1	2	4000	7.02	0.30
Junction 2	4	5000	8.08	0.24

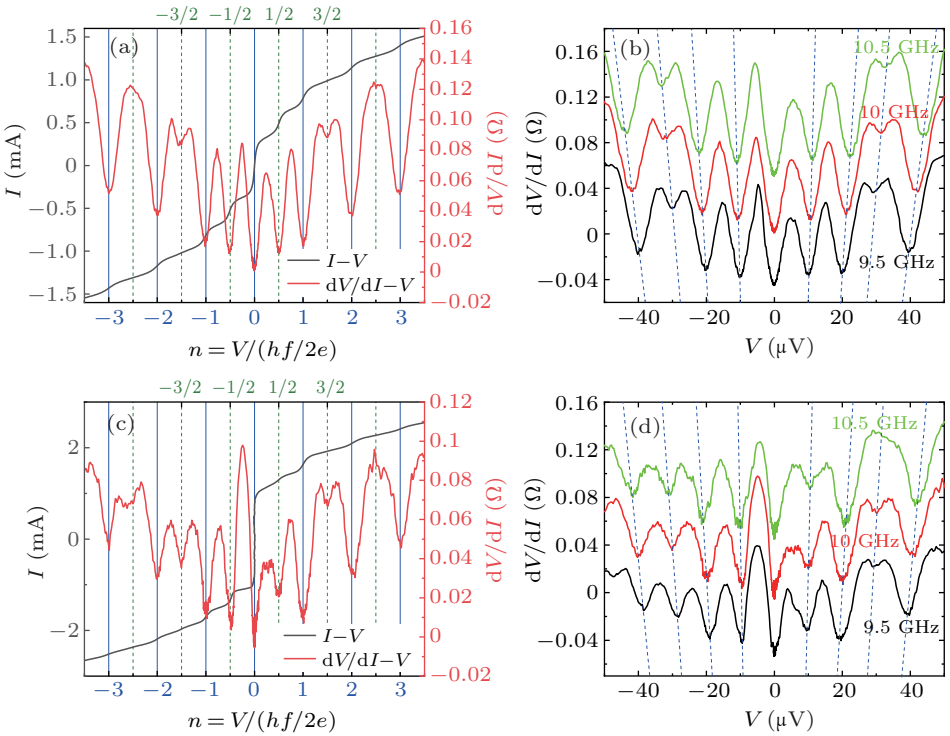


Fig. 3. (a) and (c) The I–V curves and $\mathrm{d}V/\mathrm{d}I$–V curves of junctions 1 and 2 under magnetic field and RF radiation at 2 K where clear integer and half-integer Shapiro steps can be observed. The positions of steps are labeled by vertical lines and the corresponding normalized voltages n represent the orders of steps. (b) and (d) The vertically shifted $\mathrm{d}V/\mathrm{d}I$–V curves of junctions 1 and 2 under different frequencies of RF radiation. The voltages corresponding to the steps rise with the increase of frequency.

The temperature dependence of half-integer Shapiro steps in both two junctions is also investigated. The I–V curves under fixed magnetic field and RF power at different temperatures are measured and the results are sketched in Fig. 4. The temperature test interval is 1 K and part of the I–V curves of junctions 1 and 2 are shown in Figs. 4(a) and 4(c). As the temperature goes up, the step heights (the current width ΔI of steps) of $n = 0$ steps decrease gradually, so the current positions of other steps approach zero gradually. In addition, we cannot find any half-integer steps in either junction at high temperatures. To illustrate the relationship between steps height and temperature more intuitively, the I–dV/dI curves at different temperatures are plotted into heatmaps for junctions 1 and 2 in Figs. 4(b) and 4(d). Here the white areas represent small dV/dI values, which means that there are steps and the width of the white areas represent the height of Shapiro steps. The $n = \pm 1/2$ and ± 1 steps of both two junctions are labeled by red dashed lines. It is noticed that unlike integer steps of $n = \pm 1$, which exist and change a little at all test temperatures, the half-integer steps of $n = \pm 1/2$ firstly enlarge and reach their maximum at around 4–6 K for both two junctions, then quickly become small, and finally disappear above 10 K. This demonstrates the half-integer steps have a stronger dependence on temperature than that of integer steps, which agrees with the phenomenon that the current phase relation of junctions will gradually approach standard sinusoidal form as temperature increases.[5,29] In addition, the evolution of half-integer steps' height versus temperature is not monotonic. These features are different from that of half-integer steps in ferromagnetic junctions, whose height exhibits weak correlation with temperature,[11] but are similar to that of Nb–InSb–Nb ballistic nanowire Josephson junction.[39]

The relationship between the steps' height and RF radiation power has also been researched. Here, I–V curves of junction 1 under various microwave powers at magnetic fields of 27 Oe and 31.5 Oe are shown in Figs. 5(a) and 5(c). It is obvious that a stronger RF radiation leads to a further suppression in the critical current, which is reflected in the reduction of the height of $n = 0$ step. For clarity, the corresponding heatmaps of I–dV/dI curves are plotted in Figs. 5(b) and 5(d). As with Fig. 4, the white areas suggest the existence of steps and the width of white areas represents the height of steps. When applied magnetic field is 27 Oe, clear half-integer steps of $n = \pm 1/2$ and $\pm 3/2$ can be observed and are labeled by red dashed lines. As the radiation power increases, all integer and half-integer steps except for $n = 0$ order become larger at first and then the heights of all steps start oscillating. For half-integer steps, only the first order of oscillation can be observed and then they disappear under high power of radiation. However, when junction 1 is measured at 31.5 Oe magnetic field, although clear integer steps can be observed and exhibit oscillation behaviors with the increase of radiation power, the half-integer steps do not exist at any test power. This abnormal phenomenon suggests that the existence of half-integer steps has a strong relationship with magnetic field.

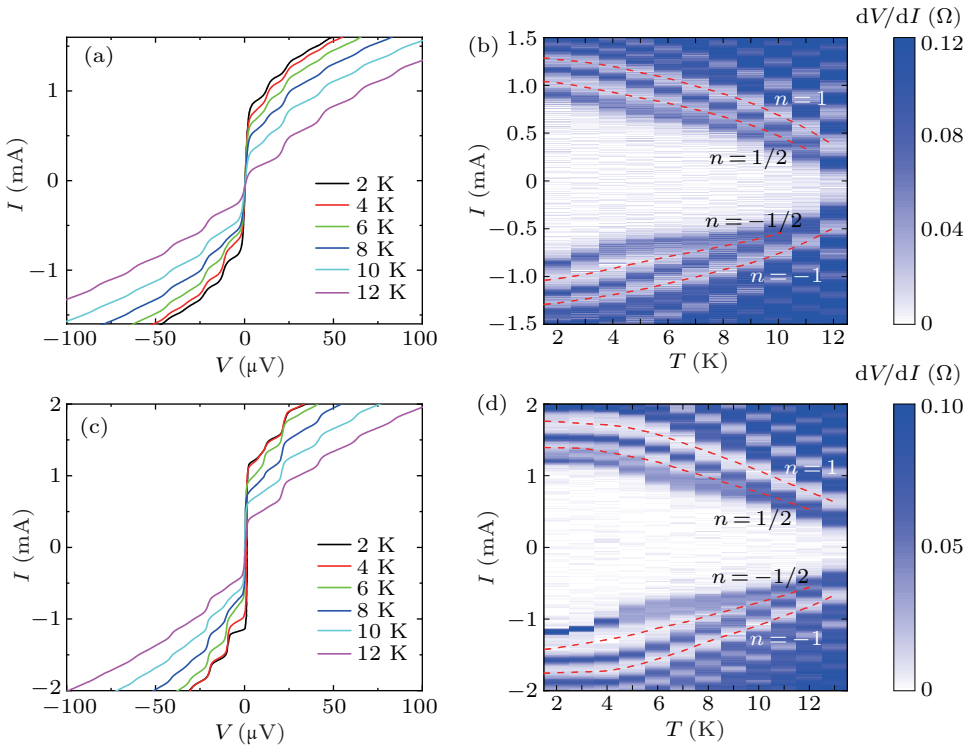


Fig. 4. (a) and (c) Selected I–V curves of junctions 1 and 2 under fixed RF radiation power and magnetic field at different temperatures. (b) and (d) Heatmaps of junctions 1 and 2's I–dV/dI curves at different temperatures. The white areas indicate integer and half-integer Shapiro steps, which are labeled by red dashed lines.

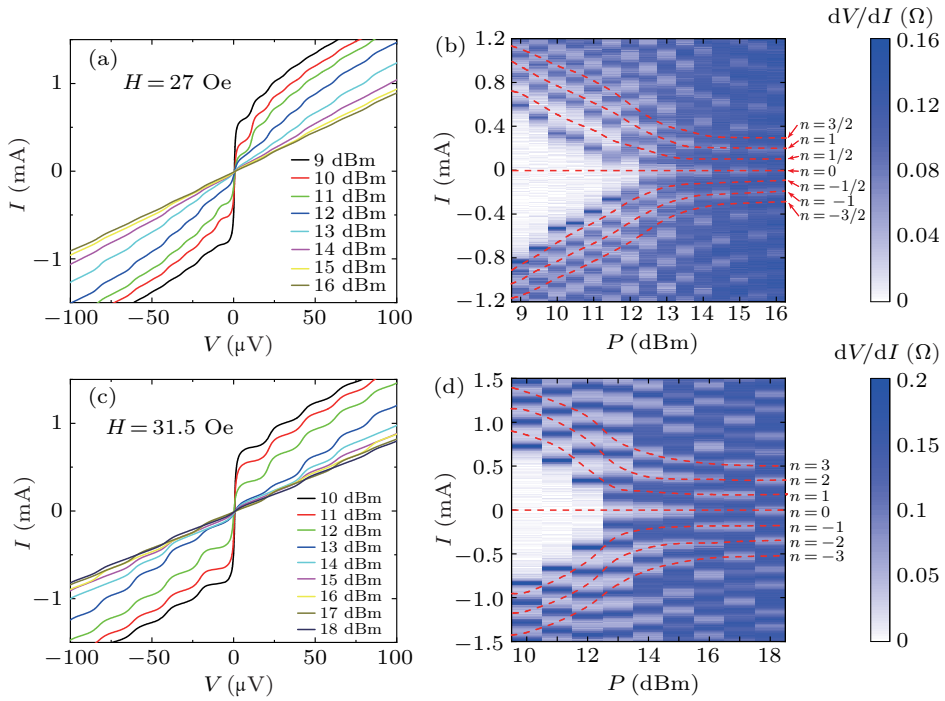


Fig. 5. (a) and (c) The I–V curves of junction 1 under different RF radiation powers at magnetic fields of 27 Oe and 31.5 Oe. Half-integer steps only appear at the magnetic field of 27 Oe. (b) and (d) Heatmaps of I–dV/dI curves whose data is collected from (a) and (c), where red dashed lines label the evolution of step heights with radiation power and oscillations can be observed.

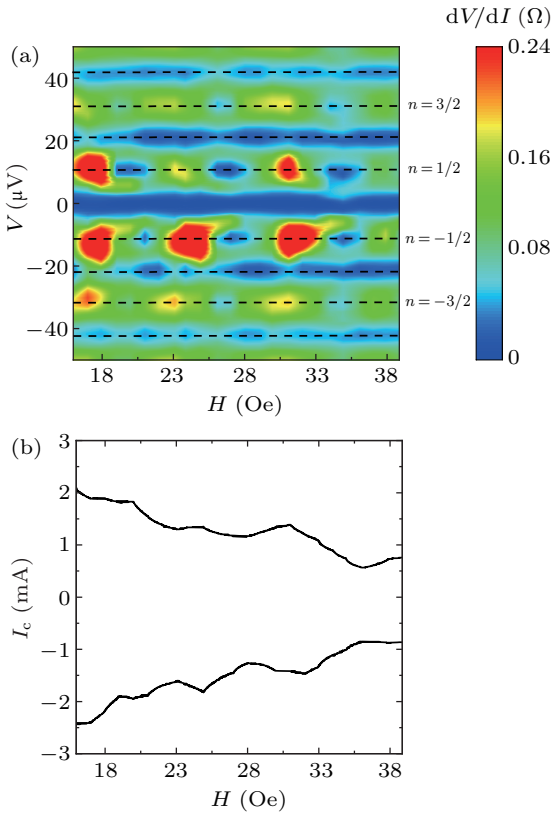


Fig. 6. (a) Colormap of V–dV/dI curves under radiation at different magnetic fields H, where blue areas indicate the appearance of steps. Half-integer steps are labeled by horizontal black dashed lines. (b) The critical current I_c that is modulated by magnetic field H for the positive and negative current directions. The data is also collected from junction 1.

To reveal the relationship between the existence of half-integer steps and applied magnetic field, transport properties of junction 1 with and without microwave radiation at different magnetic fields are measured. The V–dV/dI curves under radiation at different magnetic fields H are plotted into a colormap shown in Fig. 6(a). Here, the blue areas mean low differential resistance and indicate the appearance of steps while red areas represent steep slopes in V–I curves. Half-integer steps of $n = \pm 1/2$ and $\pm 3/2$ orders are labeled by horizontal black dashed lines. In our test magnetic field range, three half-integer steps areas are separated by quite large differential resistance parts, while the areas of integer steps behave like continuous bands. We can note that unlike integer steps which nearly exist at all test magnetic fields, the appearance of half-integer steps has a periodic relation with the magnetic field. For planar Josephson junctions, the critical current I_c is also a periodic function of H,[40] so I_c–H curves are also plotted in Fig. 6(b) for positive and negative current directions. Here, the I_c values are extracted using 1 μV as standard. We can notice the relation between the $I_c(H)$ pattern and the existence of half-integer steps. It is obviously that the half-integer steps always appear around the minimums of $I_c(H)$ curves, which is consistent with YBCO grain boundary junctions.[21,23]

4. Discussion

To our best knowledge, the similarity of the periodicity of half-integer steps modulated by magnetic field between MgB_2 He-FIB junctions and YBCO grain boundary junctions means that they may have a similar physical origin. Early *et al.* suggested that the grain boundaries of bi-crystal YBCO junctions are heterogeneous and one bi-crystal grain boundary junction is actually a 1D parallel junction array.[21] Figure 7(a) is a schematic diagram of a YBCO grain boundary junction,

where the white areas represent superconducting areas and the black areas represent normal areas. The superconducting thin film near the grain boundary is actually composed of many superconducting and non-superconducting fragments with an irregularly staggered arrangement. Only both sides of the grain boundary are superconducting fragments, a Josephson junction can exist. So many small junctions are separated by normal fragments along the grain boundary. In Fig. 7(a), red vertical solid lines label four junctions as an example and it is quite easy to understand that one grain boundary junction is actually a 1D junction array. For He-FIB junctions, it is essential to discuss the technological characteristic of He-FIB irradiation. As is shown in Fig. 7(b), although the irradiation mode of the equipment is set to line mode, the actual scan mode of He-FIB is spot-by-spot, which leads to non-uniform ions injection into the superconducting thin film along the scan direction. The lateral scattering makes the irradiated areas inside the material larger than the designed beam spot diameter. It is natural to find the similarity between grain boundary junctions and He-FIB junctions. Due to the non-uniformity of ions distribution in the irradiation area, the junction barrier created by the He-FIB is also inhomogeneous. In addition, the disappearance of half-integer Shapiro steps at high RF radiation power is in consistent with the experimental results of YBCO grain boundary junctions, whose simulation model is an unsymmetrical parallel double-junction array.[21] In conclusion, the half-integer steps in our junctions are caused by the technological characteristic of the He-FIB, which actually produces a junction with heterogeneous junction barrier which is analogous to a 1D junction array. It is reasonable to predict that similar half-integer steps can be observed in other He-FIB junctions that are made of other superconducting materials and additional studies are needed to verify this.

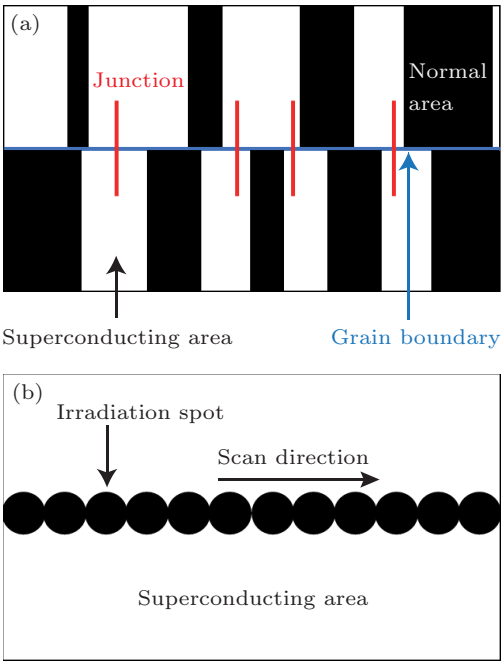


Fig. 7. (a) Schematic diagram of a YBCO grain boundary junction which is composed of many superconducting and normal fragments and is actually a 1D junction array. (b) The irradiation mode of He-FIB, which is spot-by-spot, inducing many areas with different irradiation doses.

5. Conclusion

We successfully fabricated two MgB_2 He-FIB junctions on SiC substrates, among which one is 2 μm wide with 4000 ions/nm irradiation dose and the other is 4 μm wide with 5000 ions/nm irradiation dose. Half-integer Shapiro steps appear in both of the junctions under 9.5 GHz, 10 GHz, 10.5 GHz microwave radiation. The temperature dependence of half-integer steps heights in both junctions exhibits a non-monotonic behavior. Different radiation power is applied to the junction and heights of both integer and half-integer steps exhibit oscillating behaviors. We also find that the appearance of half-integer steps exhibits a periodic function of magnetic field and the period is synchronous with that of critical current modulated by magnetic field. This feature makes us suppose that the origin of half-integer steps in MgB_2 He-FIB junctions is similar to that of YBCO grain boundary junctions. The non-uniformity of irradiation doses on the barrier of a He-FIB junction makes it behave like a 1D junction array, which induces half-integer Shapiro steps.

He-FIB technology has already shown a certain degree of universality in fabricating Josephson junctions with different superconducting materials, including low temperature simple binary compounds and high temperature complex copper oxides, which provides a platform to investigate current phase relations in different superconductors.

Data availability statement

The data that support the findings of this study are available upon reasonable request from the authors.

Acknowledgements

The work was supported by the National Natural Science Foundation of China (Grant No. 12104016) and the National Key Research and Development Program of China (Grant No. 2020YFF01014706). The authors would like to thank Lifeng Tian from Technical Institute of Physics and Chemistry Chinese Academy of Sciences and Jian Yuan from Tsinghua University for the technical guidance on He-FIB irradiation.

References

[1] Josephson B D 1962 *Phys. Lett.* **1** 251
[2] Shapiro S 1963 *Phys. Rev. Lett.* **11** 80
[3] Lehnert K, Argaman N, Blank H R, Wong K, Allen S, Hu E and Kroemer H 1999 *Phys. Rev. Lett.* **82** 1265

[4] Lee1 G H, Kim S, Jhi S H and Lee H J 2015 *Nat. Commun.* **6** 6181

[5] English C D, Hamilton D R, Chialvo C, Moraru I C, Mason N and Harlingen D J V 2016 *Phys. Rev. B* **94** 115435

[6] Ueda K, Matsuo S, Kamata H, Sato Y, Takeshige Y, Li K, Samuelson L, Xu H and Tarucha S 2020 *Phys. Rev. Res.* **2** 033435

[7] Huang Z, Elfeky B H, Taniguchi T, Watanabe K, Shabani J and Shahrjerdi D 2023 *Appl. Phys. Lett.* **122** 262601

[8] Sellier H, Baraduc C, Lefloch F and Calemczuk R 2004 *Phys. Rev. Lett.* **92** 257005

[9] Stoutimore M J A, Rossolenko A N, Bolginov V V, Oboznov V A, Rusanov A Y, Baranov D S, Pugach N, Frolov S M, Ryazanov V V and Harlingen D J V 2018 *Phys. Rev. Lett.* **121** 177702

[10] Li F, Wu L, Chen L, Zhang S, Peng W and Wang Z 2019 *Phys. Rev. B* **99** 100506

[11] Yao Y, Cai R, Yang S H, Xing W, Ma Y, Mori M, Ji Y, Maekawa S, Xie X C and Han W 2021 *Phys. Rev. B* **104** 104414

[12] Zhang Y, Lyu Z, Wang X, Zhuo E, Sun X, Li B, Shen J, Liu G, Qu F and Lü L 2022 *Chin. Phys. B* **31** 107402

[13] Hou Y L, Wang X, Sun X P and Lü L 2023 *Acta Phys. Sin.* **72** 037401 (in Chinese)

[14] Benz S P, Rzchowski M S, Tinkham M and Lobb C J 1990 *Phys. Rev. Lett.* **64** 693

[15] Sohn L L and Octavio M 1994 *Phys. Rev. B* **49** 9236

[16] Heinz E and Seidel P 1997 *J. Low Temp. Phys.* **106** 233

[17] Valizadeh A, Kolahchi M R and Straley J P 2007 *Phys. Rev. B* **76** 214511

[18] Panghotra1 R, Raes B, de Souza Silva C C, Cools I, Keijers W, Scheerder J, Moshchalkov V and de Vondel J V 2020 *Commun. Phys.* **3** 53

[19] Raes B, Tubsrinuan N, Sreedhar R, Guala D S, Panghotra R, Dausy H, de Souza Silva C C and de Vondel J V 2020 *Phys. Rev. B* **102** 054507

[20] Early E A, Clark A F and Char K 1993 *Appl. Phys. Lett.* **62** 3357

[21] Early E A, Steiner R L, Clark A F and Char K 1994 *Phys. Rev. B* **50** 9409

[22] Yang H, Ku L, Cho H, Lu J and Horng H 1994 *Physica C* **235–240** 3341

[23] Terpstra D, IJsselsteijn R P J and Rogalla H 1995 *Appl. Phys. Lett.* **66** 2286

[24] Golubov A A, Kupriyanov M Y and Ll'ichev E 2004 *Rev. Mod. Phys.* **76** 411

[25] Spanton E M, Deng M, Vaitiekėnas S, Krogstrup P, Nygård J, Marcus C M and Moler K A 2017 *Nat. Phys.* **13** 1177

[26] Buzdin A 2005 *Phys. Rev. B* **72** 100501

[27] Goldobin E, Koelle D, Kleiner R and Buzdin A 2007 *Phys. Rev. B* **76** 224523

[28] Romeo F and Luca R D 2004 *Phys. Lett. A* **328** 330

[29] Fuechsle M, Bentner J, Ryndyk D A, Reinwald M, Wegscheider W and Strunk C 2009 *Phys. Rev. Lett.* **102** 127001

[30] Cybart S A, Cho E Y, Wong T J, Wehlin B H, Ma M K, Huynh C and Dynes R C 2015 *Nat. Nanotech* **10** 598

[31] Chen Z, Li Y, Zhu R, Xu J, Xu T, Yin D, Cai X, Wang Y, Lu J, Zhang Y and Ma P 2022 *Chin. Phys. Lett.* **39** 077402

[32] Kasaei L, Melbourne T, Manichev V, Feldman L C, Gustafsson T, Chen K, Xi X X and Davidson B A 2018 *AIP Advances* **8** 075020

[33] Wang Y T, LeFebvre J C, Cho E, McCoy S J, Li H, Gu G, Kadowaki K and Cybart S A 2021 *IEEE Trans. Appl. Supercond.* **31** 1

[34] Li H, Cai H, Forman J, Cheng R, Hughes G, Walker H, Hamilton M C, Chen L, Zhang W, You L and Cybart S A 2023 *IEEE Trans. Appl. Supercond.* **33** 1

[35] Ruhtinas A and Maasilta I J 2023 arXiv:2303.17348 [cond.mat.supr.con]

[36] Chen Z, Zhang Y, Ma P, Xu Z, Li Y, Wang Y, Lu J, Ma Y and Gan Z 2024 *Chin. Phys. B* **33** 047405

[37] Xi X X, Pogrebnyakov A V, Xu S Y, Chen K, Cui Y, Maertz E C, Zhuang C G, Li Q, Lamborn D R, Redwing J M, Liu Z K, Soukiassian A, Schlom D G, Weng X J, Dickey E C, Chen Y B, Tian W, Pan X Q, Cybart S A and Dynes R C 2007 *Physica C* **456** 22

[38] Ambegaokar V and Halperin B I 1969 *Phys. Rev. Lett.* **22** 1364

[39] Iorio A, Crippa A, Turini B, Salimian S, Carrega M, Chirolli L, Zannier V, Sorba L, Strambini E, Giazotto F and Heun S 2023 *Phys. Rev. Res.* **5** 033015

[40] Rosenthal P A, Beasley M R, Char K, Colclough M S and Zaharchuk G 1991 *Appl. Phys. Lett.* **59** 3482